Joint Target Detection and Tracking Filter for Chilbolton Advanced Meteorological Radar Data Processing

Andrey Pak, Javier Correa, Martin Adams
Department of Electrical Engineering, Universidad de Chile
Daniel Clark, Emmanuel Delande, Jeremie Houssineau, Jose Franco
School of Engineering and Physical Sciences, Heriot-Watt University
Carolin Frueh
College of Engineering, Purdue University

ABSTRACT

Recently, the growing number of inactive Resident Space Objects (RSOs), or space debris, has provoked increased interest in the field of Space Situational Awareness (SSA) and various investigations of new methods for orbital object tracking. In comparison with conventional tracking scenarios, state estimation of an orbiting object entails additional challenges, such as orbit determination and orbital state and covariance propagation in the presence of highly non-linear system dynamics. The sensors which are available for detecting and tracking space debris are prone to multiple clutter measurements. Added to this problem, is the fact that it is unknown whether or not a space debris type target is present within such sensor measurements. Under these circumstances, traditional single-target filtering solutions such as Kalman Filters fail to produce useful trajectory estimates. The recent Random Finite Set (RFS) based Finite Set Statistical (FISST) framework has yielded filters which are more appropriate for such situations. The RFS based Joint Target Detection and Tracking (JoTT) filter, also known as the Bernoulli filter, is a single target, multiple measurements filter capable of dealing with cluttered and time-varying backgrounds as well as modeling target appearance and disappearance in the scene. Therefore, this paper presents the application of the Gaussian mixture-based JoTT filter for processing measurements from Chilbolton Advanced Meteorological Radar (CAMRa) which contain both defunct and operational satellites. The CAMRa is a fully-steerable radar located in southern England, which was recently modified to be used as a tracking asset in the European Space Agency SSA program. The experiments conducted show promising results regarding the capability of such filters in processing cluttered radar data.
The work carried out in this paper was funded by the USAF Grant No. FA9550-15-1-0069, Chilean Conicyt - Fondecyt grant number 1150930, EU Erasmus Mundus MSc Scholarship, Defense Science and Technology Laboratory (DSTL), U. K., and the Chilean Conicyt, Fondecyt project grant number 1150930.

1. INTRODUCTION

The precise knowledge of an orbiting object's position is crucially important in the domain of Space Situational Awareness (SSA) for two collision mitigation routines, namely, launch collision avoidance and conjunction assessment for in-orbit operational satellites. Recent accidents that contributed to significant increases in the amount of space debris within the near-Earth environment include the Chinese anti-satellite weapon test in 2007, the unintended collision of the Cosmos-2251 and Iridium 33 satellites in 2009 and more recently, the breakup of the NOAA-16 satellite in late 2015 [2]. Currently, the size of the US Space Surveillance Network (SSN) catalog of all tracked orbiting objects exceeds 20,000 items and is expected to grow to over 100,000 targets [6]. Two main sensor types that contribute to SSA information are radio-frequency (radars) and electro-optical (telescopes). Radars are primarily used for Low-Earth Orbit (LEO) object observations while telescopes are suited for the observation of higher altitude targets. Radars have been used for satellite observations since the very first satellite launch in the late 1950s.

The problem of tracking an orbital object poses a number of challenges that are not usually encountered in conventional tracking applications. These include: (a) highly non-linear motion models that are affected by a large number of external forces, e.g. third-body perturbations, atmospheric drag and solar flux; (b) limited observation times and sensor field of view and (c) birth process modeling and initial orbit determination. Furthermore, the presence of noise and clutter measurements adds complexity to the aforementioned issues.

Current state of the art tracking approaches, based on both radar and visual information, include Multiple Hypothesis Tracking (MHT) [22], Joint Probabilistic Data Association (JPDA) [3] and recently, Random Finite Sets (RFSs) [19, 20]. MHT and JPDA have been the most common multiple target tracking methods since the 1980s.

In the past decade, RFS theory has gained popularity, producing filters such as the Probability Hypothesis Density (PHD) filter [18] and Cardinalized Probability Hypothesis Density (CPHD) filter [24, 29], the Multi-target Multi-Bernoulli (MeMBer) filter [19] and the δ-Generalized Labeled Multi-Bernoulli (δ-GLMB) [28] filter. Moreover, a recent estimation framework for stochastic populations [10], applied to multi-target estimation problems, proposes a unified probabilistic description of all the system uncertainties (sensor observation process, population of targets entering/leaving the surveillance scene, target motion model, etc.) and introduces the notion of target distinguishability, allowing for the representation of a target either as an unidentified member of a larger population or as an individual track, depending on the information collected on the target so far. It is exploited in [4] on a multi-target SSA scenario, where a priori information on the number and individual states of objects is unavailable, and the number of targets and their individual trajectories are jointly estimated from the collected observations.

A number of overviews in the field of SSA propose the RFS based filters as a candidate solution for the large-scale, high-cardinality orbital object tracking scenario [13, 16]. This is because they are based on Bayesian techniques, which estimate the number of targets, the corresponding probabilities of existence, clutter rate as well as their states in a joint manner. New studies in the field of RFS based orbital object state estimation include [12, 14]. Recent developments for estimating the uncertainty of objects in orbit from ground-based sensors include [7], based on alternative parameterizations for Bayesian filtering developed in [11]. Methods for filtering and classification of objects have been developed for discriminating between different types of targets in [8].

This paper focuses on the application of the RFS Joint Target Detection and Tracking (JoTT) filter in a real orbital object radar tracking scenario. The JoTT filter, due to its lower computational complexity than its RFS multi-target counterparts, is an ideal candidate for the formulation of the space debris tracking problem based on SSA data available from Chilbolton Advanced Meteorological Radar (CAMRa) recently converted for use in SSA.

This article is organized as follows. Section 2 briefly presents the main source of data, the Chilbolton Advanced Meteorological Radar (CAMRa). Section 3 contains a brief description of a computationally tractable JoTT filter approximation, the Gaussian mixture (GM)-JoTT filter is applied to orbital object tracking. Section 4 is devoted to the results of applying the JoTT Filter to the CAMRa data, in the context of detecting and tracking active and defunct satellites. Conclusions and future work are discussed in Section 5.

2. CHILBOLTON ADVANCED METEOROLOGICAL RADAR (CAMRa)

This section introduces the CAMRa and the specifications of the data it provides. This will place into perspective the need for the JoTT filter explained later in Section 3. The radar is part of the Chilbolton atmospheric and radio research facility located near Stockbridge, UK. It is a high-power S-band meteorological radar equipped with a steerable 25m diameter dish antenna. The CAMRa was recently modified to be used as an experimental Space Surveillance and Tracking (SST) sensor, and was successfully used in the European Space Agency (ESA) "CO-VI" tracking campaign and joint UK-Australian space surveillance experiment [9, 17]. For a more detailed description on the radar specifications and configurations, the reader is referred to [5].

2.1. The CAMRa Data Format

The necessary orientation and the angular rates of the radar are computed a-priori from the Two Line Elements (TLEs) [26] of the object of interest, due to the absence of any closed-loop tracking capability. During each data acquisition step, the values of the co-polar and cross-polar signal strengths within each 75m range bin are recorded and stored. The resulting Consultative Committee for Space Data Systems (CCSDS)-compliant Tracking Data Message (TDM) file contains only one value per time step which corresponds to the highest returned signal strength in the radar's current line of sight. An example of a single data entry of the TDM file is shown in Listing 1. It contains the following fields: range (RANGE [km]), azimuth (ANGLE_1 [degrees]) and elevation (ANGLE_2 [degrees]), the co-polar (SIGNAL_STRENGTH [dB]) and cross-polar (CROSS_POLAR_SIGNAL_STRENGTH [dB]) signal strengths .

Listing 1: TDM Data entry example

```
RANGE = 2014-02-28T10:20:25.8579 638.61457294
ANGLE_1 = 2014-02-28T10:20:25.8579 11.56458378
ANGLE_2 = 2014-02-28T10:20:25.8579 16.17708397
SIGNAL_STRENGTH = 2014-02-28T10:20:25.8579 -39.53490067
CROSS_POLAR_SIGNAL_STRENGTH = 2014-02-28T10:20:25.8579 -40.40713882
```

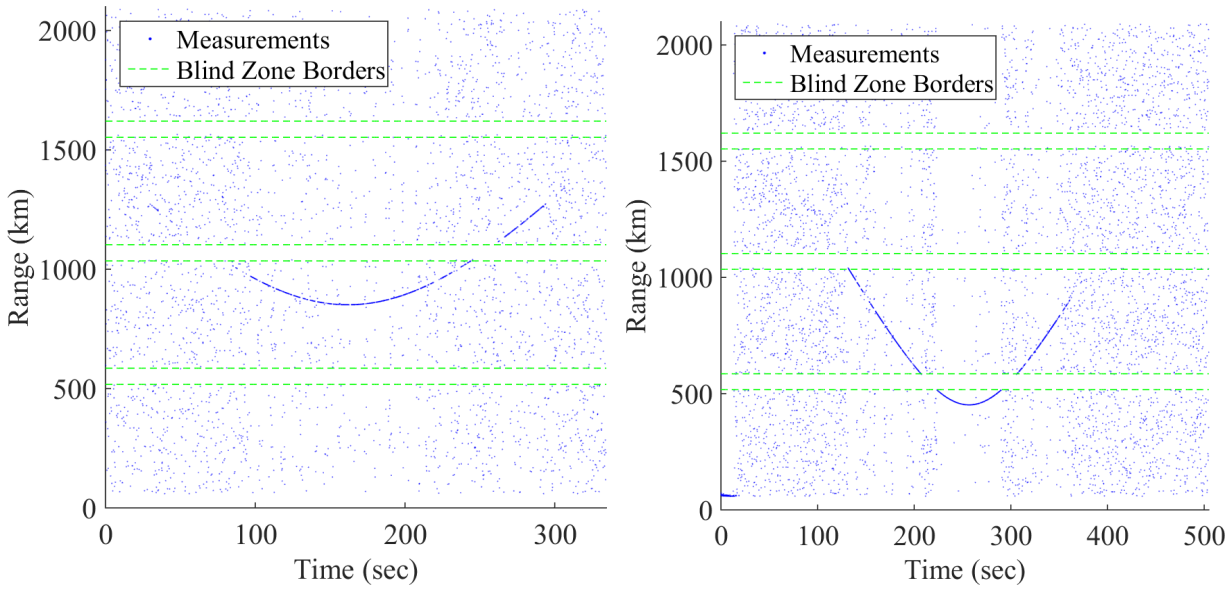

(a) Cosmos-1544 satellite pass.

(b) Cosmos-1939 satellite pass.

Fig. 1: Example CAMRa TDM datasets.

In the case of CAMRa, its data is also negatively affected by the "blind" areas at ([0.075, 517.575] + n 525) km, where n = 0, 1, 2, 3 which appear due to the sampling process in the data acquisition procedure [17]. These areas can be seen in Fig. 1.

2.2. Cell-Averaging Constant False Alarm Rate Processing

The detection of targets within radar data is based on the received power level exceeding some kind of threshold. The range-to-target decision from the TDM datasets is obtained by selecting the range bin with the highest power value from the current line of sight scan. The main shortcoming of this method is that if no target is present in the scan, the highest signal strength will correspond to some random clutter value. It is necessary to apply a different detection extraction procedure in order to overcome this problem. A constant signal strength threshold is one of the possible solutions, however, as the returned power values corresponding to the target detections vary with time and across datasets, constant thresholding does not provide a robust target detection solution.

Principled detection methods which adapt to the local noise statistics are Constant False Alarm Rate (CFAR) processors [1]. CFAR detectors are a1 family of stochastic adaptive-threshold algorithms that estimate the local noise level, in the vicinity of a range bin's power value under test, in order to derive an adaptive received power threshold for detection purposes. The Cell Averaging (CA)-CFAR processors are typically used in environments with unknown noise statistics, and will be applied here. A brief overview of CA-CFAR operation is given in Fig. 2. One can think of the CA-CFAR processor [1, Chapter 3] as a sliding window operator over the radar's A-scope that estimates the threshold based on the current range bin's neighborhood. The A-scope is the basic radar output that displays the returned signal strength as a function of range. In the case of the CAMRa data, it shows the range of the returned power values per single data acquisition step. The CA-CFAR algorithm requires two window sizes to be set. The outer window determines the size of the neighborhood which will be used in the determination of the threshold. The inner window (sometimes referred to as the guard cells) sets the size of the close vicinity that will be excluded from the evaluation. This is due to the fact that the values of the cells located near to the current cell under test are usually directly affected by its value, and do not provide a true representation of the noise.

When using the received maximum power value TDM files as a filtering input, the dataset consists of a single range measurement value per timestep accompanied by many clutter detections. On the other hand, when using the CA-CFAR detections as a filtering input, there is less clutter but possibly more than one detection per timestep. A useful filter under such conditions is the JoTT filter because all available CAMRa datasets are assumed to contain one target at most, so it precisely suits the single-target, multi-measurement nature of the processed data.

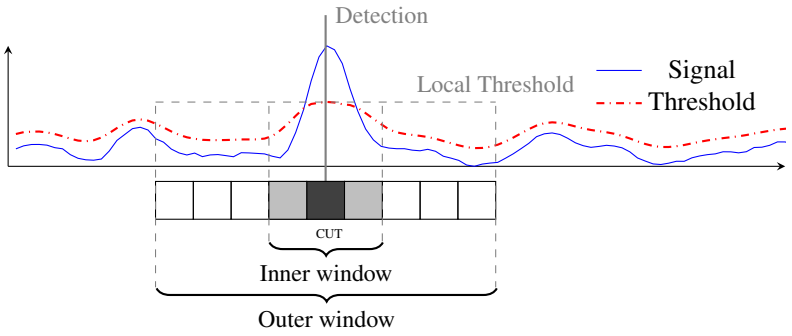

Fig. 2: CA-CFAR operation. The cell under test (CUT) neighborhood is evaluated to determine a suitable detection threshold. The CUT is shown as a black square and the corresponding guard cells are shown in grey.

3. JOINT TARGET DETECTION AND TRACKING FILTER

This section briefly describes the JoTT filter's theoretical background, state propagation model and additional steps necessary to maintain the tractability of the algorithm. The operational flow of the JoTT filter is presented in Fig. 3. The JoTT filter is an RFS-based single-target, multiple measurement filter that models the state of the target as a Bernoulli RFS [19]:

$$X = \begin{cases} 1-q, & \text{if } X = \emptyset \\ qs(\mathbf{x}), & \text{if } X = \{\mathbf{x}\} \\ 0, & \text{otherwise} \end{cases},$$

where q is the probability of target existence and $s(\mathbf{x})$ is the spatial distribution of the target.

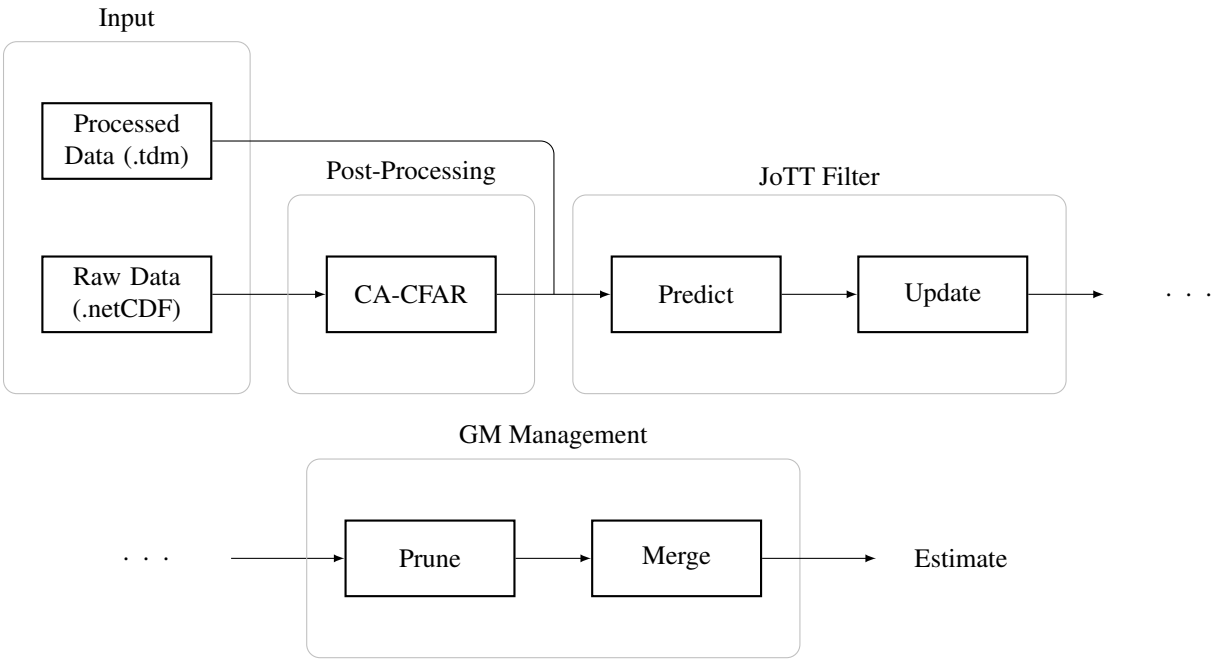

Fig. 3: The JoTT filter flow diagram. The input is either selected from the preprocessed data from the .tdm file or raw data from the .netCDF file with the subsequent CA-CFAR processing.

For the sake of computational tractability, the GM approximation of the JoTT filter will be used [23]. In the GM-JoTT filter, the spatial distribution of the target $s(\mathbf{x})$ is modeled as a weighted sum of Gaussian variables each with mean $\mathbf{m}^{(i)}$ and covariance $\Sigma^{(i)}$:

$$s(\mathbf{x}) = \sum_{i=1}^{N} w^{(i)} \mathcal{N}(\mathbf{x}, \mathbf{m}^{(i)}, \Sigma^{(i)}),$$

where $\mathcal{N}$ represents a Gaussian function with weight $w^{(i)}$. The state of the targe **x** t is represented as a six-dimensional vector in the Earth-Centered Inertial (ECI) frame [25]:

$$\mathbf{x} = \begin{bmatrix} \mathbf{p} & \mathbf{v} \end{bmatrix}^T = \begin{bmatrix} x & y & z & \dot{x} & \dot{y} & \dot{z} \end{bmatrix}^T.$$

The observations **z** are collected in the local sensor's range (ρ), azimuth (θ), elevation (ϕ) (RAZEL) frame.

$$\mathbf{z} = \begin{bmatrix} \rho & \theta & \phi \end{bmatrix}^T.$$

3.1. JoTT Filter Prediction

The prediction step of the GM-JoTT filter consists of the two following terms, which predict the probability of target existence q and its spatial distribution $s(\mathbf{x})$:

$$q_{k|k-1} = P_B(1-q_k) \qquad + P_S q_k \tag{1}$$

$$s_{k|k-1}(\mathbf{x}) = \underbrace{\frac{P_B(1-q_k)}{q_{k|k-1}} b(x)}_{\text{Birth}} + \underbrace{\frac{P_S q_k}{q_{k|k-1}} \sum_{i=1}^{N_{k-1}} w_{k-1}^{(i)} \mathcal{N}(\mathbf{x}; \mathbf{m}_{k|k-1}^{(i)}; \Sigma_{k|k-1}^{(i)})}_{\text{Survival}}, \tag{2}$$

where P_B and P_S are the probabilities of target birth and survival and $b(x)$ is the spatial distribution of the newborn components that are also modeled as a sum of Gaussian distributions. The first terms in Equations 1 and 2 correspond to the birth components while the last two are associated with the survival component. At each timestep, a single birth is performed at a range of 1000 km at the current direction of the radar. The predicted mean $\mathbf{m}_{k|k-1}$ and the covariance $\Sigma_{k|k-1}$ of each Gaussian component are obtained through the corresponding Unscented Kalman Filter (UKF) equations [15]. The propagation of the target state and sigma points is performed through the numerical integration of the state vector according to the model where only gravitational interaction between two bodies is taken into account. In this model, the gravitational acceleration a_G is represented as:

$$a_G = -\frac{\mu}{\|\mathbf{p}\|^3}, \tag{3}$$

where μ is the Earth's gravitational constant. The derivative of the state vector **x** used in the integration is then:

$$\frac{d}{dt}\mathbf{x} = \begin{bmatrix} x_4 & x_5 & x_6 & \frac{-\mu x_1}{(\sqrt{x_1^2+x_2^2+x_3^2})^3} & \frac{-\mu x_2}{(\sqrt{x_1^2+x_2^2+x_3^2})^3} & \frac{-\mu x_1}{(\sqrt{x_3^2+x_2^2+x_3^2})^3} \end{bmatrix}^T. \tag{4}$$

3.2. JoTT Filter Update

Similarly to the prediction, the JoTT filter update is performed in two steps:

$$q_k = \frac{1-\Delta_k}{1-q_{k|k-1}\Delta_k} q_{k|k-1} \tag{5}$$

$$s_k(\mathbf{x}) = \underbrace{\frac{1-P_D}{1-\Delta_k} s_{k|k-1}(\mathbf{x})}_{\text{Miss-detected components}} + \underbrace{\frac{P_D}{1-\Delta_k} \sum_{\mathbf{z}\in Z} \sum_{i=1}^{N_{k-1}} \frac{w_k^{(i)} L_k^{(i)}(\mathbf{z})}{\lambda\, \kappa(\mathbf{z})} \mathcal{N}(\mathbf{x}; \mathbf{m}_k^{(i)}; \Sigma_k^{(i)})}_{\text{Detected components}}, \tag{6}$$

where

$$\Delta_k = P_D \left[1 - \sum_{\mathbf{z} \in Z} \sum_{i=1}^{N_{k-1}} \frac{w_k^{(i)} L_k^{(i)}(\mathbf{z})}{\lambda \kappa(\mathbf{z})} \right],$$

where P_D is the probability of target detection, $L_k(\mathbf{z})$ is the Gaussian likelihood, $\lambda \kappa(\mathbf{z})$ is the clutter intensity and w_k^i is the weight of a single Gaussian component. Δ_k is a temporary variable used to calculate the normalization factor in Equations 5 and 6. In the case of the single-measurement scenario, the update equation is as follows:

$$s_k = \frac{1 - P_D}{1 - \Delta_k} s_{k|k-1}(\mathbf{x}) + \frac{P_D}{1 - \Delta_k} \sum_{i=1}^{N_{k-1}} \frac{w_k^{(i)} L_k^{(i)}(\mathbf{z})}{\lambda \kappa(\mathbf{z})} \mathcal{N}(\mathbf{x}; \mathbf{m}_k^{(i)}; \Sigma_k^{(i)}). \tag{7}$$

The first term in Equation 6 corresponds to the miss-detected components, for which the spatial distribution is not updated and is multiplied by $(1 - P_D)$ while the second term corresponds to the detected components. The updated Gaussian component mean $\mathbf{m}_{k|k}^{(}i)$ and covariance $\Sigma_{k|k}^{(i)}$ are also computed through the corresponding UKF equations.

3.3. Merging and Pruning

Within the JoTT filter, the number of elements in the Gaussian mixture grows in an exponential manner, and thus, for computational tractability, reduction mechanisms are necessary. The pruning step removes Gaussian components with weights below a pruning threshold. The weights of the remaining components are normalized thereafter. During the merging step, if a distance between two or more Gaussian components is less than a merging threshold, they are combined in a single component with a joint weight. At this stage, the Hellinger distance [21] is used as a merging criteria.

4. RESULTS

This section presents and discusses the experimental results. Since ground-truth is unavailable, filter evaluation is performed in a qualitative manner by superimposing the estimated target state onto the source data and making visual comparisons. The range filter estimates, determined from single raw measurements per timestep of the Cosmos-1544 and Cosmos-1939 satellite passes, previously shown in Fig. 1, are presented in Fig. 4. As can be seen from the plots, the JoTT filter successfully detects and continues to track the target even in the regions shown in Fig. 1, where no target-related measurements appear to be present. In both cases the filter is capable of maintaining the track continuity during the blind zones. As the probability of target survival P_S is set to one, it continues to estimate the target state until the end of the observation time. The ECI frame estimates corresponding to the Cosmos-1544 satellite pass are presented in Fig. 5.

The range estimates for the CFAR processed datasets, with multiple detections per observation, are presented in Fig 6. Both of the graphs contain the pass of the Global Precipitation Measurement (GPM) satellite at different times. As can be seen from Fig. 6(a), the initial estimation is corrected as soon as enough target-related detections are acquired. The input to the JoTT filter is the detection set produced by the CA-CFAR processor. It should be noted that after applying the CA-CFAR processor, empty measurement sets are possible. As an example, the cardinality of the CA-CFAR detections for the GPM satellite pass (Fig. 6(b)) is shown in Fig. 7. As seen from Fig. 7(b), the majority of time steps contain no detections, while the number of the detections in the remaining part (Fig. 7(a)) varies from one up to six. A useful property of the JoTT filter is that empty detection set inputs are valid, and provide useful information regarding target existence.

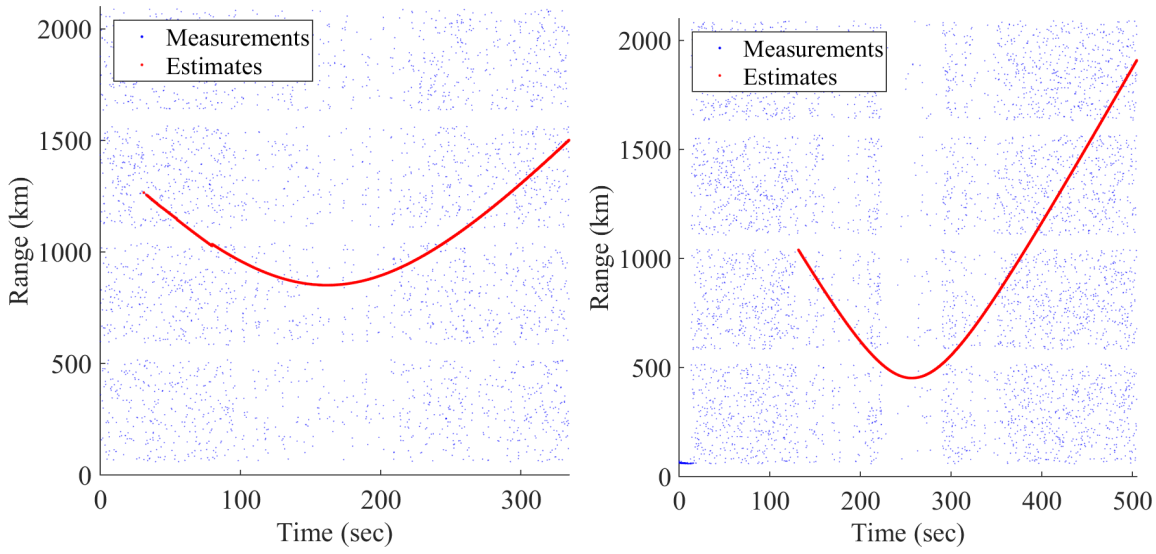

(a) Cosmos-1544 satellite pass.

(b) Cosmos-1939 satellite pass.

Fig. 4: The GM-JoTT filter range estimates. The corresponding raw datasets are shown in Fig. 1.

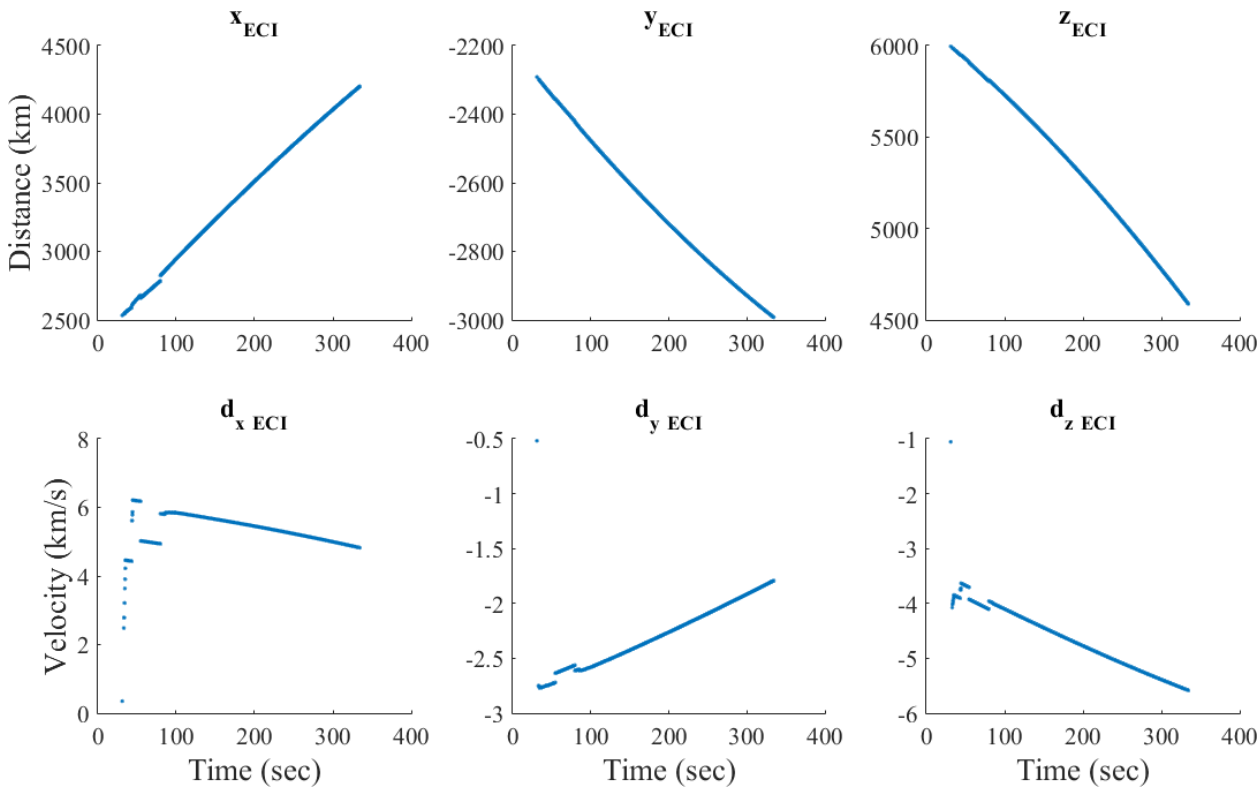

Fig. 5: The GM-JoTT filter ECI frame estimates of the Cosmos-1544 satellite pass.

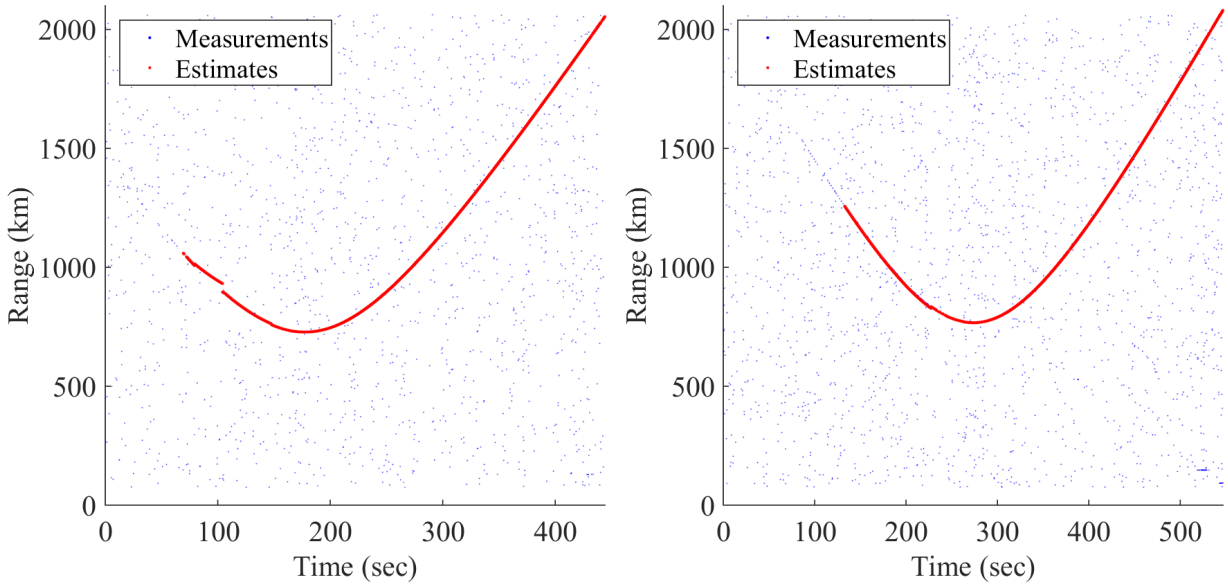

(a) GPM satellite pass (1).

(b) GPM satellite pass (2).

Fig. 6: The GM-JoTT filter range estimates, based on the CA-CFAR detector.

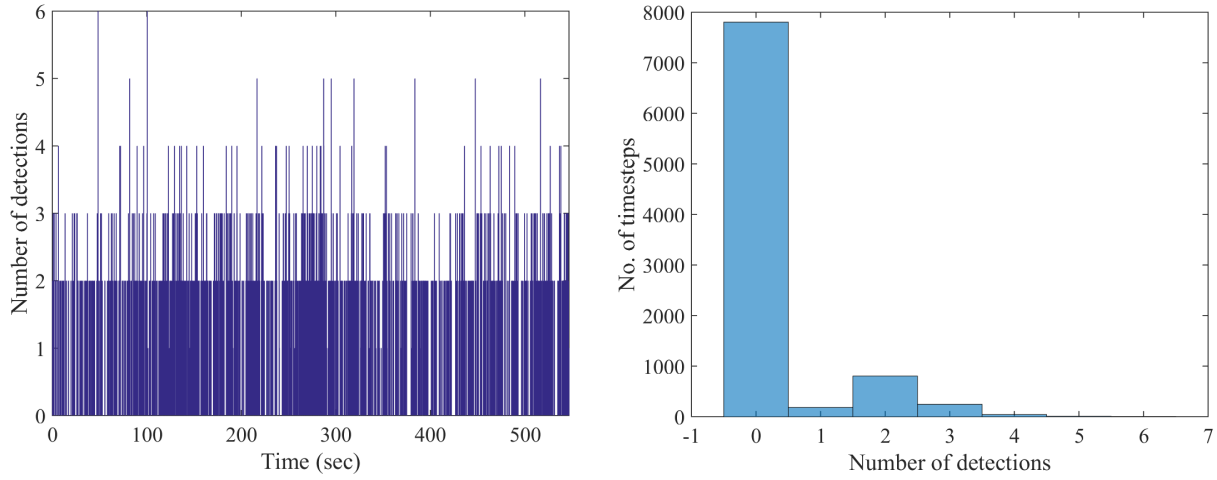

(a) Number of detections per timestep.

(b) Number of detections histogram.

Fig. 7: Detection statistics after CA-CFAR processing for the GPM satellite pass (I). The CA-CFAR parameters used are as follows: outer/inner window sizes: 100/5; false positive rate 0.1%. GPM satellite pass (see Fig. 6(b)).

5. CONCLUSIONS

This paper presented the application of the JoTT filter to the problem of state estimation of an orbital object in a real radar observation scenario. The problem of filtering raw and post-processed radar data was addressed. The JoTT filter demonstrated sufficient performance in estimating target presence and state from the CAMRa measurements. The filter provided an appropriate test bed of a single-target case that can be generalized to the multi-target case in the multi-Bernoulli filter. Future work could include the implementation of a forward-backward smoothing algorithm using methods developed in [27] for better state vector estimation as well as the introduction of appropriate Initial Orbit Determination (IOD) routines. Robust versions of the filter that can estimate the unknown probability of detection and clutter rate on-line are also being developed.

Acknowledgments

Effort sponsored by the Air Force Office of Scientific Research, Air Force Material Command, USAF, under grant number FA9550-15-1-0069. The US Government is authorized to reproduce and distribute reprints for Governmental purpose notwithstanding any copyright notation thereon. Authors would also like to express their thanks to the UK Defence Science and Technology Laboratory (DSTL) and Science and Technology Facilities Council (STFC) Chilbolton Observatory for providing the data for the article. The authors also acknowledge the Advanced Mining Technology Center (AMTC), Universidad de Chile and Conicyt, Fondecyt Project 1150930, Chile.

References

1. M. Adams, J. Mullane, E. Jose, and B.-N. Vo. *Robotic Navigation and Mapping with Radar*. Artech House, 2012.
2. National Aeronautics and Space Administration. Orbital Debris, Quarterly News, April 2016.
3. Y. Bar-Shalom, P. K. Willett, and X Tian. *Tracking and Data Fusion*. Yaakov Bar-Shalom, 11th edition, 2011.
4. E. Delande, C. Frueh, J. Houssineau, and D. E. Clark. Multi-Object Filtering for Space Situational Awareness. In *AAS Space Flight Mechanics Meeting*, 2015.
5. J. D. Eastment, D. N. Ladd, C. J. Walden, R. P. Donnelly, A. Ash, N. M. Harwood, C. Smith, J. C. Bennett, I. Ritchie, M. Rutten, et al. Technical description of radar and optical sensors contributing to joint UK-Australian satellite tracking, data-fusion and cueing experiment. In *Advanced Maui Optical and Space Surveillance Technologies Conference*, volume 1, page 12, 2014.
6. Committee for the Assessment of the U.S. Air Force Astrodynamics Standards; Aeronautics, Space Engineering Board; Division on Engineering, and Physical Sciences; National Research Council. *Continuing Keplers Quest: Assessing Air Force Space Commands Astrodynamics Standards*. National Academies Press, Washington, DC, 2012.
7. J. Franco, E. Delande, C. Frueh, J. Houssineau, and D. E. Clark. A spherical co-ordinate space parameterisation for orbit estimation. In *2016 IEEE Aerospace Conference*, pages 1–12. IEEE, 2016.
8. O. Hagen, J. Houssineau, I. Schlangen, E. D. Delande, J. Franco, and D. E. Clark. Joint estimation of telescope drift and space object tracking. In *2016 IEEE Aerospace Conference*, pages 1–10. IEEE, 2016.
9. N. M. Harwood, R. P. Donnelly, A. Ash, M. Rutten, N. Gordon, T. Bessell, J. D. Eastment, D. N. Ladd, C. J. Walden, C. Smith, et al. Joint UK-Australian Space Surveillance Target Tracking, Cueing and Sensor Data Fusion Experiment. In *Advanced Maui Optical and Space Surveillance Technologies Conference, AMOS*, 2014.
10. J. Houssineau. *Representation and estimation of stochastic populations*. PhD thesis, Heriot-Watt University, 2015.
11. J. Houssineau, D. E. Clark, S. Ivekovic, C. S. Lee, and J. Franco. A unified approach for multi-object triangulation, tracking and camera calibration. *IEEE Transactions on Signal Processing*, 64(11):2934–2948, 2016.
12. I. I. Hussein, K. J. DeMars, C. Früh, R. S. Erwin, and M. K. Jah. An AEGIS-FISST Integrated Detection and Tracking Approach to Space Situational Awareness. In *Information Fusion (FUSION), 15th International Conference on*, pages 2065–2072. IEEE, 2012.

13. B. A. Jones, D. S. Bryant, B.-T. Vo, and B.-N. Vo. Challenges of Multi-Target Tracking for Space Situational Awareness. In *Information Fusion (Fusion), 18th International Conference on*, pages 1278–1285. IEEE, 2015.

14. B. A. Jones and B.-N. Vo. A Labeled Multi-Bernoulli Filter for Space Object Tracking. In *AAS/AIAA Spaceflight Mechanics Meeting*, pages 11–15, 2014.

15. S. J. Julier and J. K. Uhlmann. Unscented filtering and nonlinear estimation. *Proceedings of the IEEE*, 92(3):401–422, 2004.

16. J. A. Kennewell and B.-N. Vo. An Overview of Space Situational Awareness. In *Information Fusion (FUSION), 16th International Conference on*, pages 1029–1036. IEEE, 2013.

17. D. N. Ladd, C. J. Walden, and M. L. Trethewey. Satellite observations using the Chilbolton radar during the initial ESA 'CO-VI' tracking campaign. In *European Space Surveillance Conference*, 2011.

18. R. P. S. Mahler. Multitarget Bayes Filtering via First-Order Multitarget Moments. *Aerospace and Electronic Systems, IEEE Transactions on*, 39(4):1152–1178, 2003.

19. R. P. S. Mahler. *Statistical Multisource-Multitarget Information Fusion*. Artech House, Inc., 2007.

20. R. P. S. Mahler. *Advances in Statistical Multisource-Multitarget Information Fusion*. Artech House, Inc,, 2014.

21. M. S. Nikulin. Hellinger distance. In M. Hazewinkel, editor, *Encyclopedia of Mathematics*.

22. D. B. Reid. An Algorithm for Tracking Multiple Targets. *Automatic Control, IEEE Transactions on*, 24(6):843–854, 1979.

23. B. Ristic, B.-T. Vo, B.-N. Vo, and A. Farina. A Tutorial on Bernoulli Filters: Theory, Implementation and Applications. *Signal Processing, IEEE Transactions on*, 61(13):3406–3430, 2013.

24. S. S. Singh, B.-N. Vo, A. Baddeley, and S. Zuyev. Filters for Spatial Point Processes. *SIAM Journal on Control and Optimization*, 48(4):2275–2295, 2009.

25. D. A. Vallado. *Fundamentals of Astrodynamics and Applications*. Microcosm Press, 4th edition, 2013.

26. D. A. Vallado, P. Crawford, R. Hujsak, and T. S. Kelso. Revisiting Spacetrack Report# 3. *AIAA*, 6753:2006, 2006.

27. B.-T. Vo, D. Clark, B.-N. Vo, and B. Ristic. Bernoulli forward-backward smoothing for joint target detection and tracking. *IEEE Transactions on Signal Processing*, 59(9):4473–4477, 2011.

28. B.-T. Vo and B.-N. Vo. Labeled Random Finite Sets and Multi-Object Conjugate Priors. *Signal Processing, IEEE Transactions on*, 61(13):3460–3475, 2013.

29. B.-T. Vo, B.-N. Vo, and A. Cantoni. The Cardinality Balanced Multi-Target Multi-Bernoulli Filter and its Implementations. *Signal Processing, IEEE Transactions on*, 57(2):409–423, 2009.